Drug absorption through a cell monolayer: A theoretical work on a non-linear three-compartment model

Niko Komin*, Raúl Toral

IFISC (Instituto de Física Interdisciplinar y Sistemas Complejos), UIB-CSIC, Campus UIB, 07122 Palma de Mallorca, Spain

ARTICLE INFO	ABSTRACT
	The subject of analysis is a non-linear three-compartment model, widely used in pharmacological absorption studies. It has been transformed into a general form, thus leading automatically to an appropriate approximation. This made the absorption profile accessible and expressions for absorption times, apparent permeabilities and equilibrium values were given. These findings allowed a profound analysis of results from non-linear curve fits and delivered the dependencies on the systems' parameters over a wide range of values. The results were applied to an absorption experiment with multidrug transporter-affected antibiotic CNV97100 on Caco-2 cell monolayers. © 2008 Elsevier B.V. All rights reserved.

1. Introduction

Orally administered drugs are mainly absorbed by the small intestine; they are mediated upon by a variety of processes (Hunter and Hirst, 1997). The drug passes from the lumen through the epithelial cells and the *lamina propria* into the blood stream (Fig. 1(left)). On its way it can be metabolised, transported away from the tract where absorption is possible or accumulate in organs other than those of treatment.

Much experimental activity aimed at analysing the kinetic aspects of the process of drug absorption has been pursued recently. For better control, a variety of *in vitro* methods of drug absorption have been developed (Balimane et al., 2000). Epithelial cell cultures can be seeded in a mono-layer, forming the contact surface between two chambers (Fig. 1(middle)) and concentrations of an applied drug can be measured over time in both chambers. Two of the well-known cell culture models are Caco-2 cells (Artursson and Borchardt, 1997; Artursson et al., 2001) and MDCK cells (Irvine et al., 1999).

Apart from a fundamental interest in understanding the basic mechanisms by which a drug is assimilated by the human body, the kinetics of drug absorption is also a topic of much practical interest. Detailed knowledge of this process, resulting in the prediction of the drug absorption profile, can be of much help in drug development stage (Eddershaw et al., 2000; Zhou, 2003). To this end,

several kinetic models for drug absorption within the body have been established (see, e.g. Yu and Amidon, 1999). In this paper, we analyse in detail a previously developed model, belonging to the category of the so-called three-compartment models (Skinner et al., 1959; Kramer et al., 1974) in which substances move between three volumes (e.g. the human organs) and active pumps are modelled by terms of non-linear fluxes. We will provide an analytical solution to an (adequate) approximation of the model, which facilitates analysis of the absorption characteristics as a whole without requiring repetitive numerical integration of the differential equations. This facilitates a fast and easy insight into how physiologically meaningful parameters influence quantities available from experiment in three-compartment models.

The paper is organised as follows: after introducing the model and presenting its solution in Section 2, we discuss the results and apply them to an antibiotic absorption study carried out with the compound CNV97100 on Caco-2 cell cultures (Section 3). Conclusions are found in Section 4. Details of the mathematical procedure are summarised in Appendix A.

2. The model and its theoretical treatment

Compartment models describe the behaviour of solutions or emulsions in connected volumes by analysing the molecule flux between them and all sources and sinks. When applied to drug absorption some specific simplifications must be made: here it is considered that two volumes (e.g. gastrointestinal lumen and blood plasma *in vivo* or apical and basolateral chamber *in vitro*) are connected through a third, *in vitro*: cellular, volume. The absorbed

* Corresponding author. Tel: +34 971 259520; fax: +34 971 173426.
E-mail address: niko@ifisc.uib-csic.es (N. Komin).
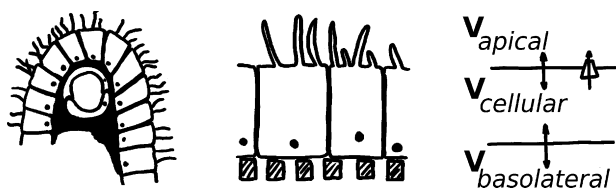
Fig. 1. Schematic view of: intestinal wall with *microvilli* and a capillary embedded in the *lamina propria* (left); epithelial cells on filter (middle); simplified mathematical model with efflux pump indicated on apical side (right).

substance should have low lipophilicity such that the unstirred water layer can be neglected. Furthermore it is assumed that the compound does not ionise and that the concentrations in the different intestinal cells of the mono-layer are equal (which is exact only if all cells have the same parameters). With these assumptions the absorption can be seen as a transport from one large volume to another through a third (the cellular) volume (Gonzalez-Alvarez et al., 2005). Fig. 1 (right) sketches the simplifications of the model. There is no spatial dependency and molecules can pass through the two cell membranes. The overall amount of drug molecules is considered to be constant, a hypothesis that assumes a closed system and that metabolism does not occur. For an *in vitro* experiment of short duration this is a reasonable assumption.

Passive transport across the membrane is mediated, to a first approximation, by the concentration gradients according to Fick's law (Fick, 1855), which specifies a linear relation between the flux of particles and the concentration gradient. When passive absorption is accompanied by energy-consuming efflux transporters, it is represented by a non-linear function term in kinetic transport equations. A variety of transporter types could be involved in the absorption of the molecules. In our work, we consider that the non-linear transporters are present only on one (the apical) cell membrane, but our results could be extended directly to the case that those transporters are located on the basolateral membrane (or even in both membranes). Incorporating both linear and non-linear terms, the time evolution of the amount of diluted molecules ($Q_{A/C/B}$) in the three compartments can be described as follows:

$$\frac{dQ_A(t)}{dt} = +Cl_{AC}\left(\frac{Q_C}{V_C} - \frac{Q_A}{V_A}\right) + \mathcal{J} \tag{1a}$$

$$\frac{dQ_C(t)}{dt} = -Cl_{AC}\left(\frac{Q_C}{V_C} - \frac{Q_A}{V_A}\right) - \mathcal{J} - Cl_{CB}\left(\frac{Q_C}{V_C} - \frac{Q_B}{V_B}\right) \tag{1b}$$

$$\frac{dQ_B(t)}{dt} = +Cl_{CB}\left(\frac{Q_C}{V_C} - \frac{Q_B}{V_B}\right) \tag{1c}$$

$$Q_0 = Q_A + Q_B + Q_C, \tag{1d}$$

where Eq. (1d) stands for conservation of the overall molecule number, Q_0. The indices denote the corresponding compartment (*Apical, Cellular, Basolateral*), $V_{A/C/B}$ are the respective volumes. The apical, cellular and basolateral concentrations are given respectively by $a = Q_A/V_A$, $c = Q_C/V_C$ and $b = Q_B/V_B$. The passive, linear, diffusion

terms are proportional to the concentration difference, being Cl_{AC} and Cl_{CB} the clearances indexed with their respective membrane index. In the equations, $\mathcal{J}$ represents the non-linear contribution due to specific efflux transporters. As it is an energy-consuming process, this can happen both along or against the gradient.

In Appendix A, we will introduce an equivalent way of writing these kinetic Eq. (1) that will demonstrate its formal similarity with some problems in the field of mechanics. This mechanical analogy will invite some approximations, consisting in a linearisation of (1), allowing us to find explicit solutions for the evolution of the number of molecules on each compartment. If approximated this way, any mass-conserving, three-compartment-model will result in a sum of three exponentials, independent from the exact form of non-linearity:

$$Q_A(t) = Q_A^{eq} - A_1 e^{-t/t_1} - A_2 e^{-t/t_2} - A_3 e^{-t/t_3} \tag{2a}$$

$$Q_B(t) = Q_B^{eq} - B_1 e^{-t/t_1} - B_2 e^{-t/t_2} - B_3 e^{-t/t_3} \tag{2b}$$

$$Q_C(t) = Q_C^{eq} - C_1 e^{-t/t_1} - C_2 e^{-t/t_2} - C_3 e^{-t/t_3} \tag{2c}$$

where t_1, t_2 and t_3 define three time-scales and Q_A^{eq}, Q_B^{eq} and Q_C^{eq} are the equilibrium asymptotic quantities of the diluted substance in each compartment. These and the constants $(A/B/C)_{(1/2/3)}$ adopt different expressions, depending on the non-linearity. If given a specific expression for the non-linear transport terms and numerical values for the parameters, one can calculate the above constants and compare the result with the numerical integration of the non-linear system (1) or with experimental data. This explicit type of solution for a Michaelis–Menten flux $\mathcal{J}$ constitutes one of the main results of this paper and is the basis for the subsequent analysis. In Section 3, we will carry out this program explicitly for the model and data taken from (Gonzalez-Alvarez et al., 2005), resulting in parameters as given in Table 2.

Experimentally, it is rare to measure the complete variation of $Q_A(t)$, $Q_B(t)$ and $Q_C(t)$ with respect to time. A typical experiment (Lentz et al., 2000; Ruiz-Garcia et al., 2002; Faassen et al., 2003; Balimane et al., 2004; Gonzalez-Alvarez et al., 2005) starts by placing an initial concentration C_0 of a drug in either the apical or in the basolateral compartment. The so-called apparent permeability $P^{app} = ((dQ/dt)/(SC_0))$, with $Q(t)$ the amount of material on the receiving side, is measured in both directions and the values are compared.

The explicit solution Eq. (2) identifies three different **characteristic time scales**, t_1, t_2 and t_3, within the evolution of these concentrations. Each one of them separates well defined regimes in the evolution of the concentrations: if time is much smaller than the characteristic time scale, the corresponding exponential term comes close to being linear; it changes exponentially at times close to it and is almost constant at much larger times. This information helps the experimenter to decide if the chosen sampling interval is adequate or not. Furthermore, it is mathematically possible to observe oscillatory behaviour in the presented system, if one of

Table 1
Time scales (when loaded apically) and apparent permeabilities predicted for different initial concentrations and different models (internal/external binding site).

C_0	Binding	t_1	t_2	t_3	P_{BA}^{app} (cm s^{-1})	P_{AB}^{app} (cm s^{-1})	$\frac{P_{BA}^{app}}{P_{AB}^{app}}$
7500	int	12.3 h	6.38 min	23.6 h	6.70×10^{-6}	6.37×10^{-6}	1.05
	ext	11.9 h	6.67 min	0.567 h	6.80×10^{-6}	4.12×10^{-6}	1.65
5000	int	12.5 h	6.27 min	23.6 h	6.73×10^{-6}	6.26×10^{-6}	1.07
	ext	11.9 h	6.67 min	0.567 h	6.86×10^{-6}	3.97×10^{-6}	1.73
1000	int	13.5 h	5.59 min	23.6 h	6.88×10^{-6}	5.57×10^{-6}	1.24
	ext	12.5 h	6.70 min	0.567 h	7.18×10^{-6}	3.10×10^{-6}	2.32
50	int	13.8 h	4.90 min	23.6 h	7.10×10^{-6}	4.88×10^{-6}	1.45
	ext	15.7 h	6.73 min	0.567 h	6.94×10^{-6}	2.07×10^{-6}	3.35

Table 2
Coefficients of solutions (2). For equilibrium solution x_{eq}, y_{eq} and coefficients $\tilde{C}_i$ and $\tilde{D}_i$ see text in Appendix A and Table 5. The numerical values are calculated for $C_0 = 7500\,\mu M$ loaded apically.

	INTRA	Numerical (μmol)	EXTRA	Numerical (μmol)
A_1	$K_M(V_C\tilde{C}_1 + V_B\tilde{D}_1)$	−8.90	$-K_M V_A\tilde{C}_1$	−5.74
A_2	$K_M(V_C\tilde{C}_2 + V_B\tilde{D}_2)$	−0.341	$-K_M V_A\tilde{C}_2$	−11.8
A_3	$K_M V_B\tilde{D}_3$	0.348	0	0
Q_A^{eq}	$Q_0 - K_M(V_C x_{eq} + V_B y_{eq})$	6.1045	$K_M V_A x_{eq}$	6.1057
B_1	$-K_M V_B\tilde{D}_1$	9.11	$-K_M V_B\tilde{D}_1$	5.88
B_2	$-K_M V_B\tilde{D}_2$	−0.0769	$-K_M V_B\tilde{D}_2$	2.82
B_3	$-K_M V_B\tilde{D}_3$	−0.348	$-K_M V_B\tilde{D}_3$	−0.0153
Q_B^{eq}	$K_M V_B y_{eq}$	8.6819	$K_M V_B y_{eq}$	8.6808
C_1	$-K_M V_C\tilde{C}_1$	−0.204	$K_M(V_A\tilde{C}_1 + V_B\tilde{D}_1)$	−0.143
C_2	$-K_M V_C\tilde{C}_2$	0.418	$K_M(V_A\tilde{C}_2 + V_B\tilde{D}_2)$	−14.7
C_3	0	0	$K_M V_B\tilde{D}_3$	0.0153
Q_C^{eq}	$K_M V_C x_{eq}$	0.21358	$Q_0 - K_M(V_A x_{eq} + V_B y_{eq})$	0.21355

the $t_{1,2,3}$ is complex. The condition for this to happen is shown in Appendix A.

We would like to stress that our way of approximating the problem has allowed us to identify these natural time scales and to find their relationship to other constants that are experimentally accessible. It appears that in many cases (one example in the next section and Table 1) one time-scale (t_2) is much smaller than the interval between measurements. Measurements of the apparent permeability are usually carried out within a time frame of between 15 and 30 min and a couple of hours (Gonzalez-Alvarez et al., 2005; Lentz et al., 2000; Yamashita et al., 2000), whereas t_2 seems to be of the order of a few minutes. Hence, measurement times satisfy $t \gg t_2$ and the exponential term e^{-t/t_2} can be neglected. Analysis of the experiments (Gonzalez-Alvarez et al., 2005) indicates that transport is mediated by transporters with an intracellular binding site. In this case, and according to Table 1, both t_1 and t_3 are much larger than the measurement times, allowing us to perform the linear approximations $e^{-t/t_1} \approx 1 - t/t_1$ and $e^{-t/t_3} \approx 1 - t/t_3$ to obtain explicit expressions for the apparent permeability:

$$P_{BA}^{app} = \frac{1}{SC_0}\left(\frac{A_1}{t_1} + \frac{A_3}{t_3}\right) \tag{3}$$

in the case that the drug is initially delivered in the basolateral side, and

$$P_{AB}^{app} = \frac{1}{SC_0}\left(\frac{B_1}{t_1} + \frac{B_3}{t_3}\right) \tag{4}$$

when the drug is delivered in the apical side. It seems that even in the case of very fast-absorbing drugs (tested for permeabilities such as those in Korjamo et al., 2007) times are well separated into those of around an hour and those of less than a minute (data not shown). However, when it occurs that the time scales are all of a similar order, one can easily extend Eqs. (3) and (4) by the required term.

Absorption of many drugs (Raviv et al., 1990) is seriously limited by P-glycoprotein (P-gp), the multidrug transporter. This particular protein is expressed on the apical membrane of intestinal epithelium cells (Troutman and Thakker, 2003a, b; Ruiz-Garcia et al., 2002). The molecule to be transported must bind with the protein and will then be "flipped" (Hunter and Hirst, 1997) onto the other side of the membrane, where it is no longer available for the "reaction". This makes its dynamics similar to enzyme reactions and is often represented by the sigmoid shape of a MICHAELIS–MENTEN reaction rate (Michaelis and Menten, 1913):

$$\mathcal{J}(Q_C) = \frac{SV_M Q_C/V_C}{K_M + Q_C/V_C}. \tag{5}$$

V_M determines the maximal reaction velocity, S is the surface area and K_M is the concentration for which the velocity extends halfway towards the maximum. In this case of an **intracellular binding** site,

the relevant variable is the concentration Q_C/V_C around the binding site of the transporter, inside the cell.

In other cases, the efflux pump possesses an **extracellular binding** site. Consequently, transport is determined by the drug concentration, Q_A/V_A, in the apical compartment and the corresponding MICHAELIS–MENTEN expression is

$$\mathcal{J}(Q_A) = \frac{SV_M Q_A/V_A}{K_M + Q_A/V_A}. \tag{6}$$

Both situations will be considered in this paper. For reasons of simplicity, we have considered that the efflux pumps depend on concentration on one of the two sides of the membrane (Ruiz-Garcia et al., 2002; Gonzalez-Alvarez et al., 2005). However, new results suggest that the transporter binding site for the molecule is inside the inner leaflet of the membrane (Hennessy and Spiers, 2007). If we consider the space inside the phospholipid bilayer to be an additional volume with two permeable walls on either side, the concentration in that volume would be between those in the adjacent volumes.

In the following section, these approximate expressions will be compared with the experimental data from Gonzalez-Alvarez et al. (2005).

3. Results

Our mathematical treatment of the evolution equations has provided us with explicit expressions for the evolution over time of the amounts $Q_{A/B/C}(t)$, Eq. (2), and the apparent permeability, Eqs. (3) and (4). In this section, we intend to determine the validity of our approach. Firstly, by comparing theoretical predictions with the full results of numerical simulations of the evolution equations, we will show that our approximate treatment has a range of validity that covers typical experimental situations.

Next, once this validity has been established, we will use our approximation to make comparisons to experimental data from an antibiotic (CNV97100, see Fig. 2) absorption study (Gonzalez-Alvarez et al., 2005). In this experiment, a pH of 7.0 was used in both the apical and the basolateral chamber to avoid any bias due to ionisation effects. If the pH were different in the two cham-
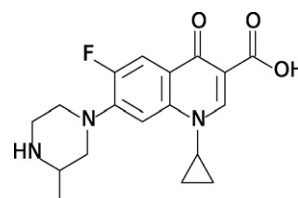

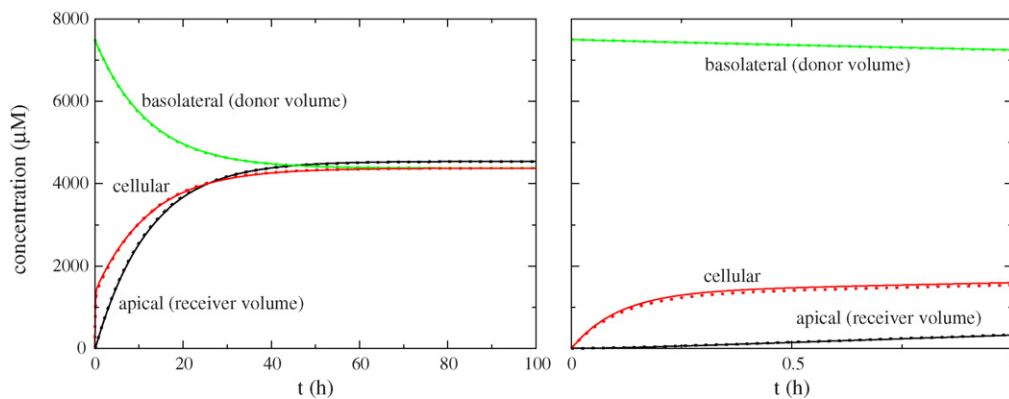**Fig. 2.** Structure of antibiotic CNV97100.

Fig. 3. Time evolution of concentrations on either side of the cells and inside. *Dotted* line: Numerical integration of Eq. (1). *Continuous* line: explicit solution Eq. (2). Parameters taken from Gonzalez-Alvarez et al. (2005), intracellular binding site with MICHAELIS–MENTEN dynamics (5) is considered. Initial concentration $C_0 = 7500\,\mu M$ is applied on the basolateral side. *Right* graph: first hour amplified.
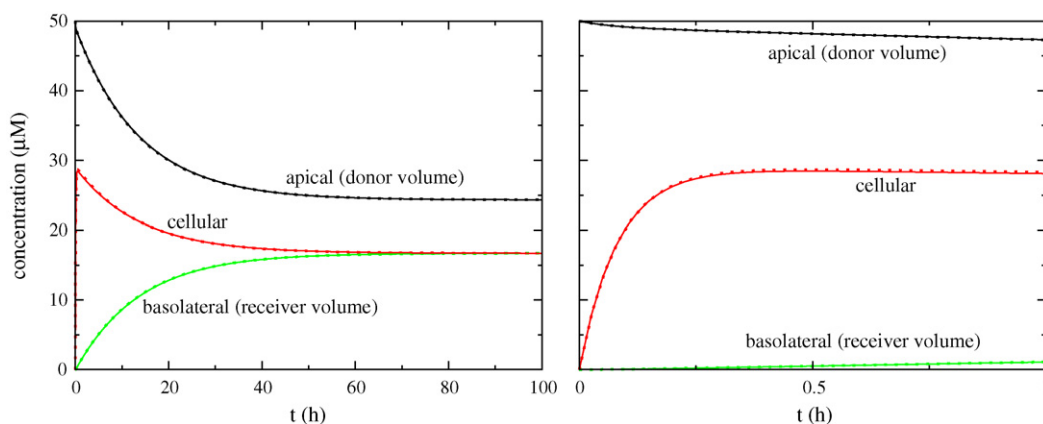

Fig. 4. Same as Fig. 3, but initial concentration 50 μM applied apically.

bers it would be necessary to include these effects into the model by estimating the fraction of ionised and non-ionised compound and to model separately the permeation of both species in both directions in each chamber. The unstirred water layer had not been considered to be the limiting diffusion step, an assumption justified by taking into account the molecular weight and the lipophilicity of CNV97100. This had been checked experimentally *in situ* in rats (Bermejo et al., 1999) and *in vitro* in Caco-2 cells (Bermejo et al., 2004). As a consequence the three compartment model with a MICHAELIS–MENTEN-type flow was chosen to be an adequate picture of the underlying processes.

Finally, we will determine the variation of the *efflux ratio*, the equilibrium concentrations and the characteristic time scales for absorption with the system parameters.

3.1. Concentration evolution and binding site location

We obtained expressions for the equilibrium amounts $Q_{A/B/C}^{eq}$ and the constants $(A/B/C)_{(1/2/3)}$ for non-linear transporters of the MICHAELIS–MENTEN-type, in cases of transport mediated by both intracellular and extracellular binding. The corresponding expressions are summarised in Table 2 as a function of parameters of the model. Using the numerical values of those parameters as derived in the absorption study of reference (Gonzalez-Alvarez et al., 2005), we can extract precise numerical values for the equilibrium amounts $Q_{A/B/C}^{eq}$ and the constants $(A/B/C)_{(1/2/3)}$. Those numerical values are also listed in Table 2. Finally, the numerical values of the time constants $t_{1/2/3}$ are listed in Table 1. Using these

numerical values, extracted from a real experiment and thus corresponding to a case of interest, we now proceed to check the accuracy of our approximation. To this end, we plotted in Figs. 3 and 4 (for two different initial conditions) the results of the direct numerical integration[1] of Eq. (1) and our approximation, Eq. (2). The most noticeable feature is that, at the scale of the figures, the two approaches are nearly indistinguishable and, in fact, the difference is of the order of the thickness of the lines. We conclude that our treatment provides a simple, yet very precise, expression for the evolution of the amounts $Q_{A/B/C}(t)$ and can be used instead of the less transparent numerical integration of the equations.

Table 1 lists the apparent permeabilities and the resulting *efflux ratios*, $P_{BA}^{app}/P_{AB}^{app}$, as obtained from Eqs. (3)–(4) in the cases of internal and external binding site and different initial concentrations. The analysis of the three time scales $t_{1/2/3}$, listed in the same table, shows that t_2 is well below the time of the first measurement (30 min) for all cases studied and the duration of experiment ($t \sim 2$ h) satisfies $t \ll t_1, t_3$, hence validating the approximations that led to Eqs. (3)–(4). The same analysis justifies the validity of the linear fit used in the experimental studies to extract the apparent permeabilities from the data. To avoid overloading the paper with too many results, we have omitted the time scales for basolateral loading since they are of similar order.

To end the comparison with experimental data, we plot the results of the CNV97100 study in Fig. 5, superimposing on the

---

[1] For this numerical integration we used a fourth-order Runge–Kutta algorithm with a time step of 1s.
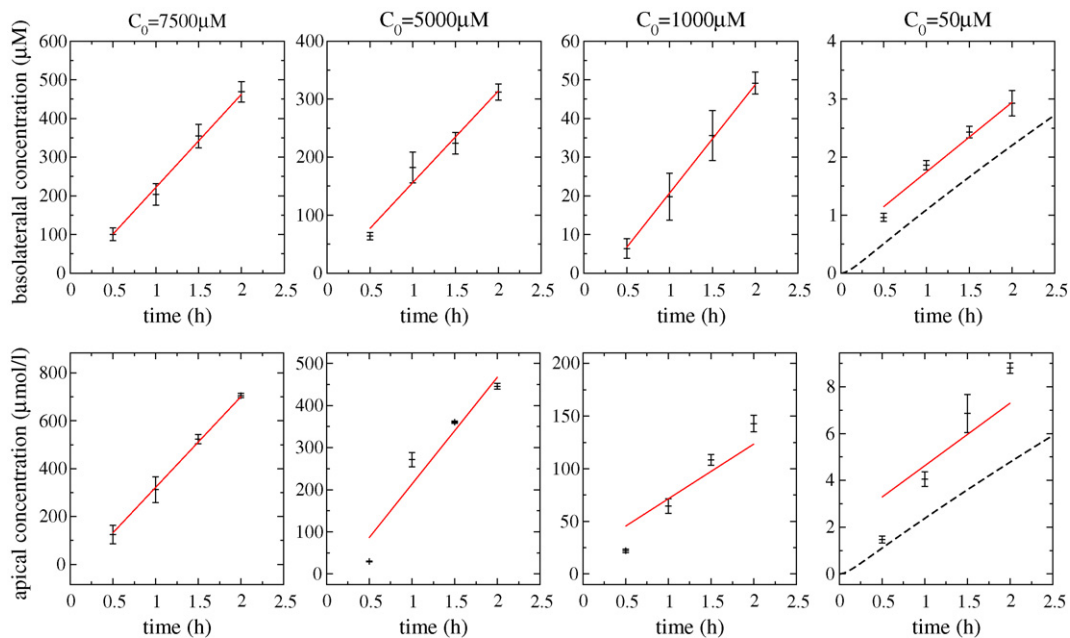
Fig. 5. Antibiotic's concentration on the receiving side. (*Top*: drug loaded in apical compartment, *bottom*: basolateral loading.) Experimental values are from CNV97100 study. The *solid* line's slope is the prediction from the theoretical solution (shown in Table 1) for intracellular binding, which was considered to be the model of best fit. The *dashed* line in the graphs on the right shows the numerical integration of the full system (1).

data a line with a slope equal to the apparent permeability from Table 1(multiplied by SC_0). If the antibiotic is loaded apically (top row in Fig. 5) the prediction of the model is good for all initial concentrations. If the loading is basolateral (bottom row); the prediction for low initial concentration underestimates the measured slope. As a consequence, the predicted efflux ratio differs from experiment at lower concentrations, which makes a more detailed analysis of this difference necessary. The MICHAELIS–MENTENkinetics used seem to provide an insuffi-

cient representation of P-gp efflux at lower initial concentrations when loaded basolaterly. The model underestimates the pump's efficiency in a basolateral to apical setup. We stress that our approximate solution still yields very accurate results for the apparent permeabilities and that this observed difference is a direct consequence of the model or the parameters used. To make this point clear, we have plotted the result of the numerical integration of (1) for the lowest concentration of 50 μM in Fig. 5. The deviation from the experimental data is clearly observable in the case of basolat-
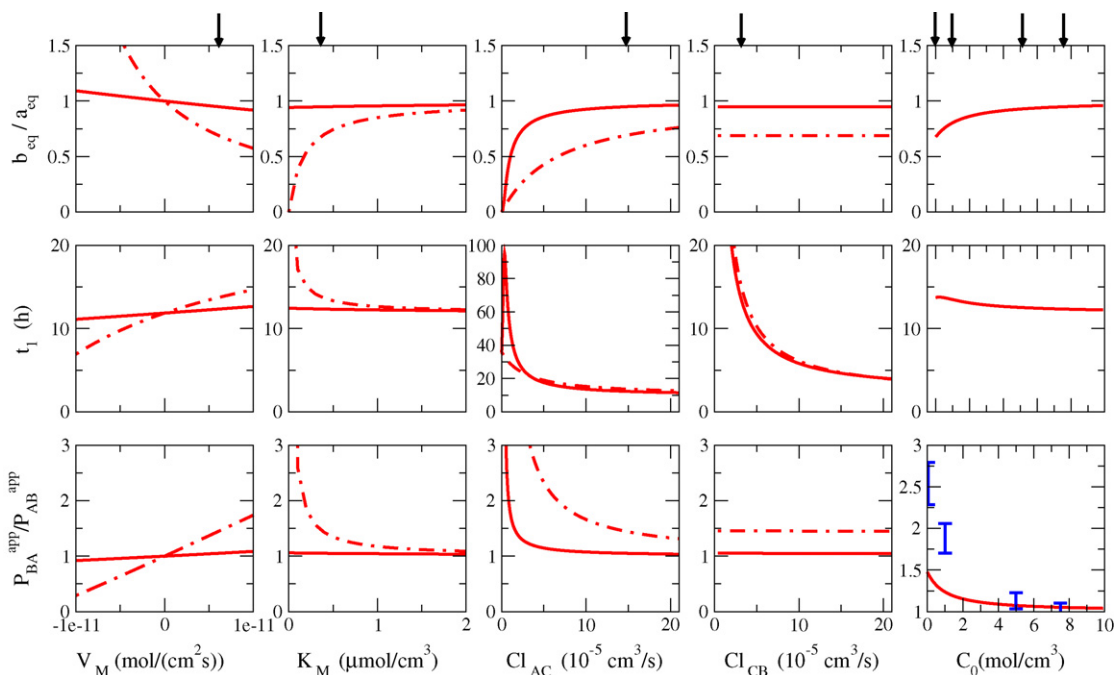

Fig. 6. Secretory pump, intracellular binding site—*Top* and *middle*: equilibrium concentration ratio (basolateral/apical) and characteristic time (both for apical loading), *bottom*: efflux ratio $P_{BA}^{app}/P_{AB}^{app}$. Dependence on V_M and K_M (transporter parameters) and clearances $Cl_{AC/CB}$. *Continuous* line: $C_0 = 7500$ μM, *dot-dashed* line: $C_0 = 50$ μM. On the very *right*: dependence on initial concentration C_0. Arrows on top mark the experimentally derived value. (Values for the respectively fixed parameters taken from Table 2.)

eral loading of the drug. Considerations of other efflux pathways in the P-gp transporter protein are found for example in Acharya et al. (2006).

3.2. Parameter dependence

Once we had determined the validity of our approach, we wished to use the explicit expressions to determine the dependence on the system parameters of some quantities which are of experimental interest. Here lies one of the strengths of our solution: in Fig. 6, we plot the characteristic time scale for absorption t_1, the equilibrium concentration ratio on both cell sides b_{eq}/a_{eq} and the efflux ratio $P_{BA}^{app}/P_{AB}^{app}$ as a function of the clearances Cl_{AC} and Cl_{CB}, the pump parameters V_M and K_M and the initial concentration of drug C_0. Analytic formulas give access to these results much easier than repetitive integration throughout parameter space plus extracting the data from the resulting trajectories.

Again, for reasons of simplicity, we have limited our presentation to the case of a secretory pump located apically with intracellular binding site; the best model according to analysis by Gonzalez-Alvarez et al. (2005). As observed in this figure, an increase in the initial concentration C_0 implies a decrease in the characteristic time t_1 from a finite value to a minimum value, limiting t_1 to a certain range. Raising C_0 increases the equilibrium concentration ratio b_{eq}/a_{eq}. Although this ratio varies significantly, steady concentration in the basolateral site, b_{eq}, shows a good linear dependence with C_0 (not shown in the figure). Note that the efflux ratio $P_{BA}^{app}/P_{AB}^{app}$ also decreases with increasing initial concentration, a feature supported by the experimental data, although the theoretical values deviate from the experimental results at low concentrations, a fact already discussed in the previous section. The clearance Cl_{CB} of the membrane where the pump is not situated has no influence on the equilibrium concentration and efflux ratios, but an increase of Cl_{CB} decreases the characteristic time t_1, indicating a faster transport of the drug. On the other hand, an increase in the clearance Cl_{AC} of the cell membrane where the pump is located has the effect of decreasing the efflux ratio and increasing the equilibrium concentration ratio. For large initial concentrations, $C_0 = 7500\,\mu M$, the characteristic time t_1 shows interesting behaviour with Cl_{AC} since it first increases and then decreases, indicating very slow drug absorption for some intermediate values of the clearance.

At large concentrations, the three quantities analysed show small dependence with respect to the pump parameters V_M and K_M, since the corresponding curves are almost flat. This makes it difficult to extract from the data accurate values of the pump parameters at those large concentrations. This suggests that lower concentrations would allow for a better experimental determina-

tion of the pump parameters – a practise used by experimentalists – however, we have to take into account, as discussed above, that the accuracy of the model might worsen with decreasing concentration. In the graph, we have included negative values for V_M, which is equivalent to a change in the flow direction of the pump.

Apart from these considerations, analysis of parameter dependency is the first step towards examining the propagation of errors into the experimentally available quantities. For example, it is clear from Fig. 6 (third and fourth column), that small differences in Cl_{AC} would be nearly unnoticed, due to the rather flat curve around its measured value (marked by the black arrow on top of the figures). On the other hand, a small change in Cl_{CB} yields a big variation of time scale t_1. More detailed investigations of errors and how they bias the results have been left aside for subsequent investigations.

4. Discussion

Three-compartment models are widely used in drug absorption studies. The one treated here consists of a linear part, representing passive absorption (for example through cell membranes), and a non-linear part which models other means of transport, such as ABC-transporter proteins embedded into the cell membrane. In this work, we have shown a way to transform this model into the picture of a *ball in a well* (Fig. 7), which is a general form of equations facilitating analysis of mathematical structure. The lowest point of the "well" gives the value of the **equilibrium concentration** after saturation of the process. With an adequate approximation, one can derive the **absorption profile** as the sum of three exponentials and identify their **characteristic time scales** dividing the process into phases of linear change, non-linear fluxes and saturation. In the phase of a near-linear profile we can provide explicit expressions for the **apparent permeability**, a quantity usually measured in experiments.

These are general results which we used on a showcase system, where the non-linear transport is described by a Michaelis–Menten profile—a common model of transporter proteins (Sharma et al., 2002; Volk and Schneider, 2003; Mizuarai et al., 2004). The approach presented in this paper make efflux ratio and time scales accessible. Both *apical* and *basolateral* drug loading can be treated by changing the initial conditions; we furthermore considered the possibilities of *intra* cellular as well as extracellular binding sites. We analysed the importance of each physiological parameter in a wide range of values.

The presented results may contribute to a better understanding of the absorption process and to explaining differing observations in identical experimental setups from a more fundamental basis. Knowledge of parameter dependencies, a fundamental analysis of errors (confidence interval) and their consequences becomes possible. This has been left aside for later studies. The most promising experimental setups can furthermore be predicted by treating a newly proposed model in the same way.
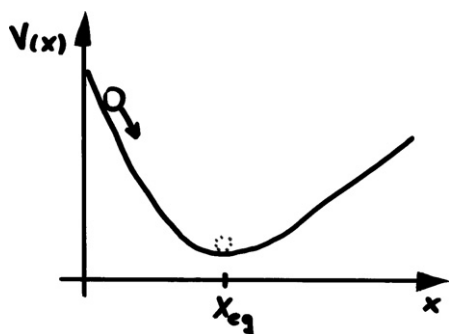
Acknowledgements

Fig. 7. Visualisation of the particle-potential picture. The position of the "ball" represents the concentration which will eventually end up in the minimum.

Table 3
Coefficients for Eq. (8) using parameter values from Gonzalez-Alvarez et al. (2005).

Parameter	INTRAcellular	Numerical	EXTRAcellular	Numerical
a_{11}	$-\left[\frac{V_B}{V_C} + \frac{Cl_{AC}}{Cl_{CB}}\left(\frac{V_B}{V_C} + \frac{V_B}{V_A}\right)\right]$	-213.8	$-\frac{Cl_{AC}}{Cl_{CB}}\left(\frac{V_B}{V_C} + \frac{V_B}{V_A}\right)$	-173.1
a_{12}	$\frac{V_B}{V_C}\left(1 - \frac{Cl_{AC}}{Cl_{CB}}\frac{V_B}{V_A}\right)$	-209.8	$-\frac{Cl_{AC}}{Cl_{CB}}\frac{V_B^2}{V_A V_C}$	-250.4
a_{13}	$\frac{Cl_{AC}}{Cl_{CB}}\frac{V_B V_I}{V_A V_C}c_0$	$2.220 \times 10^8 V_I C_0$	$\frac{Cl_{AC}}{Cl_{CB}}\frac{V_B V_I}{V_A V_C}c_0$	$2.220 \times 10^8 V_I C_0$
a_{21}	1	1	$-\frac{V_A}{V_C}$	-27.10
a_{22}	-1	-1	$-\left(\frac{V_B}{V_C} + 1\right)$	-41.65
a_{23}	0	0	$c_0 \frac{V_I}{V_C}$	$3.604 \times 10^8 V_I C_0$
γ	$-\frac{SV_M}{Cl_{CB}K_M}\frac{V_B}{V_C}$	-79.41	$\frac{SV_M}{Cl_{CB}K_M}\frac{V_B}{V_A}$	2.930
Parameter				Numerical
Γ_0	$-a_{11} - a_{22} = \frac{V_B}{V_C} + \frac{Cl_{AC}}{Cl_{CB}}\left(\frac{V_B}{V_C} + \frac{V_B}{V_A}\right) + 1$			214.8
α	$a_{12}a_{23} - a_{13}a_{22} = \frac{Cl_{AC}}{Cl_{CB}}\frac{V_B V_I}{V_A V_C}c_0$			$2.220 \times 10^8 V_I C_0$
β	$a_{11}a_{22} - a_{12}a_{21} = \frac{Cl_{AC}}{Cl_{CB}}\frac{V_B}{V_A V_C}(V_A + V_B + V_C)$			423.6

Appendix A

We will now give an overview of the used mathematical methods used and show the explicit solutions in the following subsections.

The conservation law Eq. (1d) reduces the number of independent variables from three to two concentrations. In other words, the system described by first-order differential Eq. (1) only has two degrees of freedom. This implies that it can be replaced by a single differential equation of second order of the form

$$\ddot{x} = -\Gamma(x)\dot{x} + F(x). \tag{7}$$

Variable x represents a rescaled concentration in one of the compartments (the cellular compartment if $\mathcal{J}$ depends on Q_C, as when using (5), and the apical compartment if $\mathcal{J}$ depends on Q_A, as when using (6)); the speed, $\dot{x}$, and acceleration, $\ddot{x}$, are, respectively, the first and second derivatives of x with respect to a rescaled time s, and $\Gamma(x)$ and $F(x)$ are functions to be described below.

A qualitative understanding of these dynamics can be had by acknowledging that the previous equation corresponds to the equation of motion (NEWTON's second law) for the position x of a particle of unit mass upon which a force $F(x)$ and a friction, proportional to the particle speed $\dot{x}$ act. The force $F(x)$ and the friction coefficient $\Gamma(x)$ contain all of the parameters of the system as well as the particular form of the non-linear flux (Eq. (10)).

If we now introduce the potential function $V(x)$ from which the force derives as $F(x) = -(dV/dx)$, the evolution of x can be visualised as the relaxation of a ball rolling downwards within a well of shape $V(x)$ under the combined effects of gravity and friction. It is known from mechanics that the particle will eventually stop at the minimum of the potential (stable equilibrium state) and that relaxation towards this final state will proceed via damped oscillations or monotonously, depending on the relative strength of the friction and potential contributions. Fig. 7 visualises this *ball-in-a-well* approach. For very general non-linear transporters, including the MICHAELIS–MENTEN form, Eqs. (5) and (6), used in this paper, the corresponding potential function $V(x)$ displays a single minimum, although its exact shape depends both on the linear and the non-linear terms in Eq. (1).

Once this mechanical simile has been realised, an approximation appears quite natural: the potential $V(x)$ is replaced by the parabolic approximation around its minimum, equilibrium, value x_{eq}, i.e. approximate $V(x) \approx V(x_{eq}) + \frac{\omega^2}{2}(x - x_{eq})^2$. Similarly, the friction coefficient is replaced by its value at this minimum $\Gamma(x) \approx \Gamma(x_{eq}) =$ Γ_{eq}. With these approximations, NEWTON's Eq. (7) becomes the linear equation $\ddot{x} = -\Gamma_{eq}\dot{x} - \omega^2(x - x_{eq})$, which describes the damped pendulum of frequency ω. The solution of this equation, as found in many elementary books of mechanics, can be written as the sum of exponential functions of time. One can then undo the change of variables and write the solution in full as done above (Eq. 2)

A.1. Parameters and simplifications for three-compartment system

The conservation law (1d) allows the elimination of one of the three equations of the set (1a-1c). We have chosen to eliminate either Q_A or Q_C, depending on whether the non-linearity depends on Q_C or Q_A, respectively. More precisely: if $\mathcal{J} = \mathcal{J}(Q_C)$, we define the dimensionless normalised concentration $x(t) = ((Q_C(t))/(V_C\mathcal{N}))$ where $\mathcal{N}$ is a normalisation constant with units of concentration to be specified later; in the other case, when $\mathcal{J} = \mathcal{J}(Q_A)$, we define $x(t) = ((Q_A(t))/(V_A\mathcal{N}))$. In both cases, we also define $y(t) = ((Q_B(t))/(V_B\mathcal{N}))$. The initial drug concentration $C_0 = Q_0/V_I$ (being $V_I = V_A$ or $V_I = V_B$ according to whether the drug is initially loaded on the apical or the basolateral volume, respectively) is also rescaled to $c_0 = (C_0/\mathcal{N})$. We finally define a rescaled dimensionless time variable $s = (Cl_{CB}/V_B)t$. It turns out that, with these definitions, the resulting two-degree system can be written in the common form:

$$\dot{x}(s) = \frac{dx(s)}{ds} = a_{11}x + a_{12}y + a_{13} + j(x) \tag{8a}$$

$$\dot{y}(s) = \frac{dy(s)}{ds} = a_{21}x + a_{22}y + a_{23}. \tag{8b}$$

with $j = (V_B/(Cl_{CB}V_A\mathcal{N}))\mathcal{J}(Q_A)$ in one case, and $j = -(V_B/(Cl_{CB}V_C\mathcal{N}))\mathcal{J}(Q_C)$ in the other. The dimensionless constants a_{ij} depend on the clearances, volumes, overall concentration, as specified in Table 3.

By differentiating $\dot{x}(s)$ with respect to s using Eq. (8a) and, in the resulting expression, replacing $\dot{y}(s)$ by Eq. (8b) and $y(s)$ by its isolation from Eq. (8a), we get the form (7):

$$\ddot{x} = -\Gamma(x)\dot{x} + F(x), \tag{9}$$

with friction coefficient $\Gamma(x)$ and force $F(x)$ given by:

$$\Gamma(x) = \Gamma_0 - j'(x), \quad F(x) = \alpha - \beta x - a_{22}j(x). \tag{10}$$

Γ_0, α and β are dimensionless, positively defined constants, whose relation to the coefficients a_{ij} are also detailed in Table 3.

Table 4
Experimental parameters drawn from Gonzalez-Alvarez et al. (2005) used for the calculations.

Parameter	Measured value
Cl_{AC}	14.49×10^{-5} cm^3/s
Cl_{CB}	3.528×10^{-3} cm^3/s
V_M	6.17×10^{-12} mol/(cm^{2}s)
K_M	0.376 mol/cm^3
S	4.2 cm^2
V_A	2 cm^3
V_B	3 cm^3
V_C	0.0738 cm^3

A.2. Coefficients in case of MICHAELIS–MENTEN efflux transporter

This presentation has so far been very general. In the case of the MICHAELIS–MENTEN form for the non-linear efflux transport function $\mathcal{J}$, formulas (5) or (6), we identify K_M as a characteristic concentration and simply adopt the normalisation constant $\mathcal{N} = K_M$. Therefore, the current is

$$j(x) = \gamma \frac{x}{1+x} \tag{11}$$

where γ is written up in Table 3. The friction coefficient and force are

$$\Gamma(x) = \Gamma_0 - \frac{\gamma}{(1+x)^2}, \quad F(x) = \alpha - \beta x - \gamma a_{22} \frac{x}{1+x}. \tag{12}$$

Note that the initial concentration C_0 is contained only in α and that the influence of the efflux transporter is found completely in γ. Γ_0, α and β are independent of the location of the pump. The values used for numerical calculations are taken from (Gonzalez-Alvarez et al., 2005) and can be seen in Table 4.

The potential from which the force $F(x) = -(dV(x)/dx)$ derives is:

$$V(x) = (-\alpha + \gamma a_{22})x + \frac{\beta}{2}x^2 - \gamma a_{22} \ln(1+x). \tag{13}$$

The equilibrium concentration x_{eq} is the minimum of the potential, obtained by setting the force in Eq. (12) equal to zero. In the present case of a MICHAELIS–MENTEN-type non-linearity, the solution is obtained without using any further approximations or simplifications other than stated for the original model:

$$x_{eq} = \frac{\alpha - \beta - \gamma a_{22} + \sqrt{4\alpha\beta + (\alpha - \beta - \gamma a_{22})^2}}{2\beta}. \tag{14}$$

Inserted into (8b) the equilibrium value for $y(s)$ is the solution of $\dot{y}(s) = 0$:

$$y_{eq} = -\frac{a_{21}x_{eq} + a_{23}}{a_{22}} \tag{15}$$

Table 5
Coefficients of dimensionless solution Eqs. (18) and (21).

$\tilde{C}_1$	$\left(x_0 - x_{eq} + \tau_2\left(a_{11}x_0 + a_{12}y_0 + a_{13} + \gamma\frac{x_0}{1+x_0}\right)\right)\frac{\tau_1}{\tau_1-\tau_2}$
$\tilde{C}_2$	$x_0 - x_{eq} - \tilde{C}_1$
$\tilde{D}_1$	$-\frac{a_{21}\tilde{C}_1\tau_1}{a_{22}\tau_1+1}$
$\tilde{D}_2$	$-\frac{a_{21}\tilde{C}_2\tau_2}{a_{22}\tau_2+1}$
$\tilde{D}_3$	$y_0 - y_{eq} - \tilde{D}_1 - \tilde{D}_2$

Through the conservation law one gets z_{eq}:

$$z_{eq} = \frac{Q_0}{V_z\mathcal{N}} - x_{eq}\frac{V_x}{V_z} - y_{eq}\frac{V_B}{V_z}, \tag{16}$$

where, to unify notation, we have labelled the volumes' meaning $V_x = V_C$ and $V_z = V_A$ for intracellular binding, and $V_x = V_A$ and $V_z = V_C$ for extracellular binding.

A.3. The linearised model

The potential $V(x)$, Eq. (13), has a single minimum and it can be approximated by a parabola around this minimum $V(x) = V_{eq} + (1/2)V_{eq}''(x - x_{eq})^2$. The second derivative with respect to x is

$$V''(x_{eq}) = \omega^2 = \beta + \frac{a_{22}\gamma}{(1+x_{eq})^2}. \tag{17}$$

The approximated and original potentials are drawn in Fig. 8 in the case of apical loading of a system with intracellular binding site. From this figure, it can be seen that the parabolic form constitutes an excellent approximation for a wide range of initial concentrations C_0.

Furthermore, we also approximate the friction coefficient $\Gamma(x)$ by its value at equilibrium $\Gamma_{eq} = \Gamma_0 - (\gamma/((1+x_{eq})^2))$. The resulting linear differential equation $\ddot{x} = -\Gamma_{eq}\dot{x} - \omega^2(x - x_{eq})$ has the solution (Boyce and DiPrima, 2001):

$$x(s) = \tilde{C}_1 e^{-s/\tau_1} + \tilde{C}_2 e^{-s/\tau_2} + x_{eq} \tag{18}$$

with time constants:

$$\tau_1 = \frac{2}{\Gamma_{eq} - \sqrt{\Gamma_{eq}^2 - 4\omega^2}} \quad \text{and} \quad \tau_2 = \frac{2}{\Gamma_{eq} + \sqrt{\Gamma_{eq}^2 - 4\omega^2}} \tag{19}$$

The coefficients $\tilde{C}_1$ and $\tilde{C}_2$ are determined by the initial conditions x_0 and $\dot{x}_0$, the latter being determined through Eq. (8b) by x_0 and y_0 as $\dot{x}_0 = a_{11}x_0 + a_{12}y_0 + a_{13}j(x_0)$. The resulting formulas are summarised in Table 5. The initial values x_0 and y_0 depend on the particular model used. For example, for intracellular binding we have $x_0 = ((Q_C(t=0))/(V_C K_M)) = 0$ and $y_0 = ((Q_B(t=0))/(V_B K_M))$. This latter value, in turn, has to be adjusted according to where the drug is loaded: for apical loading $y_0 = 0$, while for basolateral loading $y_0 = (C_0/K_M)$. Note that τ_1 and τ_2 will be complex if $\Gamma_{eq} < 2\omega$.
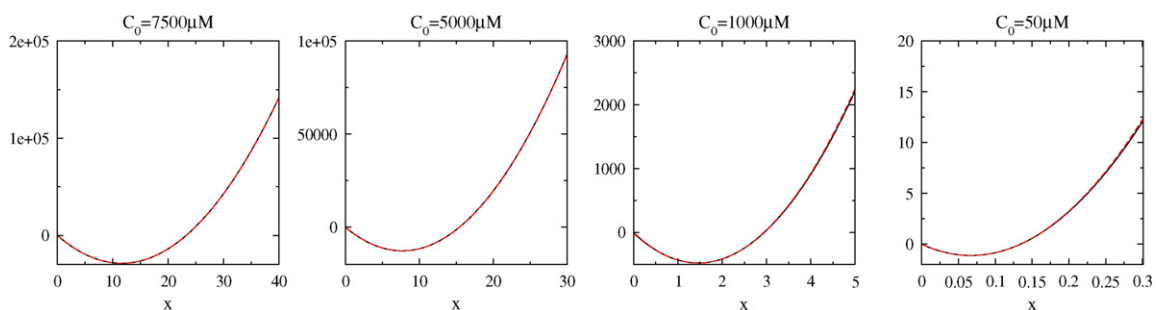

Fig. 8. *Continuous* line: Original potential Eq. (13), *dashed* line: approximated parabola. For different amounts of loaded drug. Differences are of the order of the line width.

In this case, the system would relax to the steady state by performing damped oscillations. However, for the values of the parameters drawn from experiments, this case does not arise, τ_1 and τ_2 are positive real numbers and the decay to the equilibrium state is governed by real exponentials.

The time evolution of y can be obtained by a direct integration of the linear Eq. (8b):

$$y(s) = e^{a_{22}s} \left[y_0 + \int_0^s ds' e^{-a_{22}s'}(a_{21}x(s') + a_{23}) \right] \qquad (20)$$

which yields

$$y(s) = \tilde{D}_1 e^{-s/\tau_1} + \tilde{D}_2 e^{-s/\tau_2} + \tilde{D}_3 e^{-s/\tau_3} + y_{eq}. \qquad (21)$$

with a new time constant:

$$\tau_3 = -\frac{1}{a_{22}} \qquad (22)$$

and coefficients $\tilde{D}_{1/2/3}$, whose relation to other constants is detailed in Table 5. The evolution of $z(s)$ is obtained by means of the conservation law. Finally, when we undo the changes of variables we obtain coefficients as given in Table 2 and together with Eq. (19) we derive Eq. (2). It is worth recalling that the time scales in real units are

$$t_1 = \frac{V_B}{Cl_{CB}}\tau_1, \quad t_2 = \frac{V_B}{Cl_{CB}}\tau_2, \quad t_3 = \frac{V_B}{Cl_{CB}}\tau_3. \qquad (23)$$

References

Acharya, P., Thuy, T.T., Polli, J.W., Ayrton, A., Ellens, H., Bentz, J., 2006. P-glycoprotein (p-gp) expressed in a confluent monolayer of hmdr1-mdckii cells has more than one efflux pathway with cooperative binding sites. Biochemistry 45, 15505–15519.

Artursson, P., Borchardt, R.T., 1997. Intestinal drug absorption and metabolism in cell cultures: Caco-2 and beyond. Pharmaceutical Research 14 (12), 1655–1658.

Artursson, P., Palm, K., Luthman, K., 2001. Caco-2 monolayers in experimental and theoretical predictions of drug transport. Advanced Drug Delivery Reviews 46, 27–43.

Balimane, P.V., Chong, S., Morrison, R.A., 2000. Current methodologies used for evaluation of intestinal permeability and absorption. Journal of Pharmacological and Toxicological Methods 44, 301–312.

Balimane, P.V., Patel, K., Anthony, M., Chong, S., 2004. Utility of 96-well caco-2 cell system for increased throughput of p-gp screening in drug discovery. European Journal of Pharmaceutics and Biopharmaceutics 58, 99–105.

Bermejo, M., Avdeef, A., Ruiz, A., Nalda, R., Ruell, J.A., Tsinman, O., González, I., Fernández, C., Sánchez, G., Garrigues, T.M., Merino, V., 2004. Pampa–a drug absorption in vitro model: 7. comparing rat in situ, caco-2, and pampa permeability of fluoroquinolones. European Journal of Pharmaceutical Sciences 21 (4), 429–441.

Bermejo, M., Merino, V., Garrigues, T.M., Delfina, J.M.P., Mulet, A., Vizet, P., Trouiller, G., Mercier, C., 1999. Validation of a biophysical drug absorption model by the patqsar system. Journal of Pharmaceutical Sciences 88 (4), 398–405.

Boyce, W.E., DiPrima, R.C., 2001. Elementary Differential Equations and Boundary Value Problems. John Wiley & Sons Inc.

Eddershaw, P.J., Beresford, A.P., Bayliss, M.K., September 2000. Adme/pk as part of a rational approach to drug discovery. Drug Discovery Today 5 (9).

Faassen, F., Vogel, G., Spanings, H., Vromans, H., 2003. Caco-2 permeability, p-glycoprotein transport ratios and brain penetration of heterocyclic drugs. International Journal of Pharmaceutics 263, 113–122.

Fick, A., 1855. Ueber diffusion. Annalen der Physik 170, 59–86.

Gonzalez-Alvarez, I., Fernandez-Teruel, C., Garrigues, T., Casabo, V., Ruiz-García, A., Bermejo, M., December 2005. Kinetic modelling of passive transport and active efflux of a fluoroquinolone across caco-2 cells using a compartmental approach in nonmem. Xenobiotica.

Hennessy, M., Spiers, J., 2007. A primer on the mechanics of p-glycoprotein the multidrug transporter. Pharmacological Research 55, 1–15.

Hunter, J., Hirst, B.H., 1997. Intestinal secretion of drugs. the role of p-glycoprotein and related drug efflux systems in limiting oral drug absorption. Advanced Drug Delivery Reviews 25, 129–157.

Irvine, J.D., Takashi, L., Lockhart, K., Cheong, J., Tolan, J.W., Selick, H.E., Grove, J.R., 1999. Mdck (madin-darby canine kidney) cells: a tool for membrane permeability screening. Journal of Pharmaceutical Sciences 88 (1), 28–33.

Korjamo, T., Kemiläinen, H., Heikkinen, A.T., Mönkkönen, J., 2007. Decrease in intracellular concentration causes the shift in k_m value of efflux pump substrates. Drug Metabolism amd Disposition 35 (9), 1574–1579.

Kramer, W.G., Lewis, R.P., Tyson, C.C., Forester, W.F., Visconti, J.F., Wanke, L.A., Boxenbaum, H.G., Reuning Jr., R.H., 1974. Pharmacokinetics of digoxin: Comparison of a two- and a three-compartment model in man. Journal of Pharmacokinetics and Biopharmaceutics 2 (4), 299–312.

Lentz, K.A., Polli, J.W., Wring, S.A., Humphreys, J.E., Polli, J.E., 2000. Influence of passive permeability on apparent p-glycoprotein kinetics. Pharmaceutical Research 17 (12).

Michaelis, L., Menten, M., 1913. Die kinetik der invertinwirkung. Biochemische Zeitschrift, 333–369.

Mizuarai, S., Aozasa, N., Hidehito, K., 2004. Single nucleotide polymorphisms result in impaired membrane localization and reduced atpase activity in multidrug transporter abcg2. International Journal of Cancer 109, 238–246.

Raviv, Y., Pollard, H., Bruggemann, E., Pastan, I., Gottesman, M., 1990. Photosensitized labeling of a functional multidrug transporter in living drug-resistant tumor cells. Journal of Biological Chemistry 7, 3975–3980.

Ruiz-Garcia, A., Lin, H., Plá-Delfina, J.M., Hu, M., 2002. Kinetic characterization of secretory transport of a new ciprofloxacin derivative (cnv97100) across caco-2 cell monolayers. Journal of Pharmaceutical Sciences 91 (12), 2511–2519.

Sharma, K.G., Mason, D.L., Liu, G., Rea, P.A., Bachhawat, A.K., Michaelis, S., 2002. Localization, regulation, and substrate transport properties of bpt1p, a saccharomyces cerevisiae mrp-type abc transporter. Eukaryotic Cell 1 (3), 391–400.

Skinner, S.M., Clark, R.E., Baker, N., Shipley, R.A., 1959. Complete solution of the three-compartment model in steady state after single injection of radioactive tracer. American Journal of Physiology 196, 238–244.

Troutman, M.D., Thakker, D.R., August 2003. Efflux ratio cannot assess p-glycoprotein-mediated attenuation of absorptive transport: Asymmetric effect of p-glycoprotein on absorptive and secretory transport across caco-2 cell monolayers. Pharmaceutical Research 20 (8), 1200–1209.

Troutman, M.D., Thakker, D.R., August 2003. Novel experimental parameters to quantify the modulation of absorptive and secretory transport of compounds by p-glycoprotein in cell culture models of intestinal epithelium. Pharmaceutical Research 20 (8), 1210–1224.

Volk, E.L., Schneider, E., September 2003. Wild-type breast cancer resistance protein (bcrp/abcg2) is a methotrexate polyglutamate transporter. Cancer Research 63, 5538–5543.

Yamashita, S., Furubayashi, T., Kataoka, M., Sakane, T., Sezaki, H., Tokuda, H., 2000. Optimized conditions for prediction of intestinal drug permeability using caco-2 cells. European Journal of Pharmaceutical Sciences 10, 195–204.

Yu, L.X., Amidon, G.L., 1999. A compartmental absorption and transit model for estimating oral drug absorption. International Journal of Pharmaceutics 186, 119–125.

Zhou, H., 2003. Pharmacokinetic strategies in deciphering atypical drug absorption profiles. The Journal of Clinical Pharmacology 43, 211–227.